



HAL
open science

Multiphysic FEMLAB modelisation to evaluate mid-infrared photonic detector performances

Yvan Cuminal, Philippe Christol, Jean-Baptiste Rodriguez, André Joullié

► **To cite this version:**

Yvan Cuminal, Philippe Christol, Jean-Baptiste Rodriguez, André Joullié. Multiphysic FEMLAB modelisation to evaluate mid-infrared photonic detector performances. Nov 2005, pp.109-112. hal-00102053v1

HAL Id: hal-00102053

<https://hal.science/hal-00102053v1>

Submitted on 29 Sep 2006 (v1), last revised 30 May 2007 (v4)

HAL is a multi-disciplinary open access archive for the deposit and dissemination of scientific research documents, whether they are published or not. The documents may come from teaching and research institutions in France or abroad, or from public or private research centers.

L'archive ouverte pluridisciplinaire **HAL**, est destinée au dépôt et à la diffusion de documents scientifiques de niveau recherche, publiés ou non, émanant des établissements d'enseignement et de recherche français ou étrangers, des laboratoires publics ou privés.

MULTIPHYSIC FEMLAB MODELISATION TO EVALUATE MID-INFRARED PHOTONIC DETECTOR PERFORMANCES.

Y. Cuminal^{(a)*}, P. Christol^(b), J.B Rodriguez^(b) and A. Joullie^(b)

^(a)Laboratoire des Sciences des Matériaux et d'Automatique (LASMEA), Université Clermont II,
UMR CNRS 6602, 63177 Aubière (France).

^(b)Centre d'Electronique et de Micro-optoélectronique de Montpellier (CEM2), Université de Montpellier-II, UMR CNRS
5507, 34095 Montpellier (France).

1. Introduction :

Infrared photonic detectors operating in the mid infrared region find applications in pollution monitoring, high-speed infrared imaging systems and free space telecommunications. Currently, the dominant infrared detector technologies are based on HgCdTe or InSb photovoltaic devices^[1]. However, because of their narrow band gap, these devices show at room temperature (RT) high dark reverse current leading to small zero-bias resistance detector-area product R_0A , which significantly restrict the getting of high ambient temperature performances. Consequently, there is a need for new uncooled high performance detector systems and antimonide-based (Sb-based) semiconductor quantum structures could be an alternative of the well-established technologies^[2].

The main objective of this communication is to demonstrate that, thanks to a multiphysic FEMLAB modelisation, it is possible to simulate the electro-optic device behaviour in order to determine the optimised Sb-based structure for RT detection.

2. Modelling equations :

The electro-optic modelling is based upon the coupled resolution of the Poisson equation (eq. 1), the equation of continuity for electrons and holes (eq. 2) and the equations of continuity under illumination (eq. 3a and 3b). In these equations the three dependent variables used for the modelling are the electrostatic potential (Ψ), the electron and hole concentrations (n and p , respectively).

$$-\nabla \cdot (\varepsilon \cdot \nabla \Psi) = q \cdot (p - n + N) \quad (1)$$

$$-\nabla \cdot J_n = -q \cdot R_{SRH} \quad ; \quad -\nabla \cdot J_p = q \cdot R_{SRH} \quad (2)$$

$$\frac{\partial n}{\partial t} = Gop(z) - \frac{\Delta n}{\tau_n} + \frac{1}{q} \cdot \nabla J_n \quad (3a)$$

$$\frac{\partial p}{\partial t} = Gop(z) - \frac{\Delta p}{\tau_p} - \frac{1}{q} \cdot \nabla J_p \quad (3b)$$

Where q is the elementary charge, and ε the effective dielectric constant of the material; N represents fixed charges associated to the ionised acceptors and donors; J_n and J_p are the electron and

hole current densities, respectively; τ_n and τ_p are the lifetime of electrons and holes.

In the eq. (3a) and (3b), $Gop(z)$ is the optical generation rate given by^[3] :

$$G_{op}(y) = \alpha \cdot \Phi_0 \cdot \exp[-\alpha \cdot (y - y_0)] \quad (4)$$

while $\Delta n = n - n_0$ and $\Delta p = p - p_0$

Φ_0 is the incident photons stream on the photodetector surface. n_0 and p_0 are equilibrium carrier densities and α is the absorption coefficient of the considered material.

In the eq. 2, the current densities for electrons and holes can be expressed as the sum of the conduction and diffusion currents :

$$J_n = -q \cdot n \cdot \mu_n \cdot \nabla \Psi + q \cdot D_n \cdot \nabla n \quad (5)$$

$$J_p = -q \cdot p \cdot \mu_p \cdot \nabla \Psi - q \cdot D_p \cdot \nabla p \quad (6)$$

Where μ_n and μ_p are the carrier mobility, and D_n and D_p are the diffusion coefficients for electrons and holes.

The term R_{SRH} is the generation / recombination Shockley-Read-Hall rate for deep level trap :

$$R_{SRH} = \frac{n \cdot p - n_i^2}{\tau_p \cdot (n + n_1) + \tau_n \cdot (p + p_1)} \quad (7)$$

where n_1 and p_1 are the electrons and hole densities determined for the trap energy level, n_i is the intrinsic carriers concentration.

In the case of a trap level in the middle of the band gap : $n_1 = p_1 = n_i = N_c \exp(-E_g / 2kT)$ according to the Fermi's equation.

The R_{SRH} expression means that if $n \cdot p \neq n_i^2$, typically in a space charge zone of a polarised diode, there is generation ($n \cdot p > n_i^2$) or recombination ($n \cdot p < n_i^2$) of electron-hole pairs in this area.

If we assume that the permanent state is reached, then $\frac{\partial p}{\partial t} = \frac{\partial n}{\partial t} = 0$ and equations (3a) & (3b) become:

$$\frac{1}{q} \cdot \nabla J_n = Gop(z) - \frac{\Delta n}{\tau_n} \quad (8)$$

$$\frac{1}{q} \cdot \nabla J_p = Gop(z) - \frac{\Delta p}{\tau_p} \quad (9)$$

* Corresponding author Email : cuminal@lasmea.univ_bpclermont.fr

3. Modelised structures :

The calculation has been performed on a n^+np Sb-based photodetector (Fig.1). As shown, this structure is constituted by a GaSb p type substrate covered by an over doped GaSb buffer. The active zone is realised by a quantum nanostructure based on InAs/GaSb superlattice (SL) designed to have a cut-off wavelength at $5.4 \mu\text{m}$ [4], at the beginning of the mid-infrared domain. The length and the doping level of this layer are not specified because used as modeling parameters. In order to obtain a good electrical contact an InAs high doping level n^+ type layer is deposited at the top of the structure. An example of the calculated energy bands of this structure is done Fig.2.

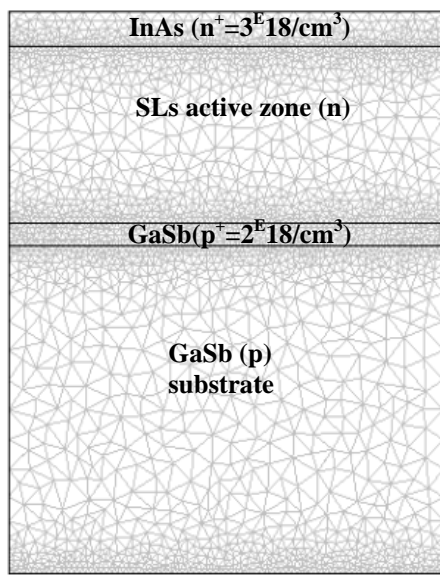


Fig.1: Schematic view of the n^+np Sb-based photodetector. Example of meshing used for modelling.

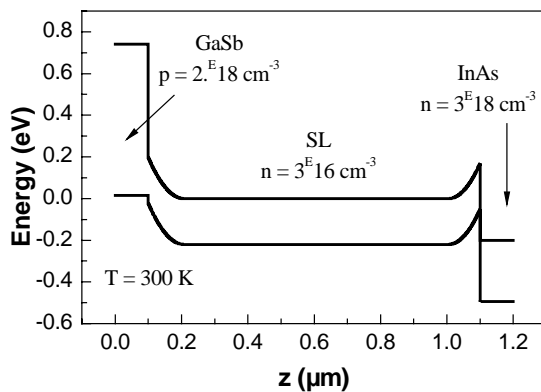


Fig.2: Calculated band energies diagram of modelised photodetector.

4. Modelling parameters :

Equations (1) (2) (8) and (9) were solved for the photodetector structure (Fig.1). The calculation was done with a parametric non-linear multiphysic solver using electrostatic and diffusion FEMLAB modules. This modelling is based upon the same method than the semiconductor diode model presented in the FEMLAB model library [5].

For this resolution we assume the continuity of electric potential and electric field between each layer. For boundaries far from the component active zone, the normal electric field component and the carrier densities are taken equal to zero. At the electric contacts (boundaries in touch with metal), electric potential were considerate as fixed and we suppose an infinite recombination velocity on these surfaces.

For the resolution, we also suppose that the permanent state is reached, that is suppressing any temporal dependence in the equations (3). Finally, because the p doped GaSb is not transparent in the mid-infrared wavelength range, we have considered that the photodiode is illuminated by the n doped side, leading to $y_0 = 0$ in eq.4.

The used parameters for materials are given in Table 1. For the SL active zone, the energy gap (E_g), the absorption coefficient (α) and the intrinsic carrier concentration (n_i) were deduced from optical measurement [6]. To take in account the anisotropy of the quantum active zone, the diffusion coefficient was define as anisotropic parameter with a lower value in y direction (perpendicularly to the surface of the photodetector structure).

An example of meshing used for this modelling is given Fig.1. As shown, the meshing is denser where the doping levels vary quickly, at the boundaries and near contacts. These meshing parameters were also adapted to the structure geometry and to obtain a convergent solution.

	GaSb	InAs	active zone
E_g (meV)	725	356	225
α (cm^{-1})	0	1E3	5E3
n_i (cm^{-3})	1.5E12	1E15	2.11E15
ϵ_r	15.69	15.15	16.24
μ_n (cm^2/Vs)	3E3	1E4	500
μ_p (cm^2/Vs)	200	100	100
τ_n (s)	1E-9	2E-9	2E-9
τ_p (s)	2E-9	1E-9	2E-9

Table 1: Material parameters used for modelling.

5. Results and discussion :

We present in this part the main modelling results obtained with the structure previously presented. The theoretical performances of the photodetector for RT operation are calculated in terms of R_0A product ($R_0A = A.(dV/dI)_{V=0}$ where A is the photodiode surface) and of quantum efficiency η because the main figure of merit of the photodetector *the specific detectivity* D_{λ}^* is directly proportional of these two values (eq. 10).

$$D_{\lambda}^* = R(\lambda) \sqrt{\frac{R_0A}{4kT}} \quad (10)$$

where k is the Boltzmann constant and $R(\lambda)$ is the responsivity of the photodetector in A/W taking into account the quantum efficiency by the following expression :

$$R(\lambda) = \frac{\eta q}{hv} = \frac{\lambda \eta}{1.24} \quad (11)$$

where λ is the wavelength in μm corresponding to a photon energy hv .

The calculations were made varying the active zone length from $0.25\mu m$ to $3\mu m$ for three different doping levels ($n = 3.10^{16} cm^{-3}; 1.10^{17} cm^{-3}; 3.10^{18} cm^{-3}$).

5.a R_0A product :

Fig.3 represents the RT current-voltage characteristic obtained for the three active zone doping level. For this calculation we considered a typical active zone length $d=1.5\mu m$.

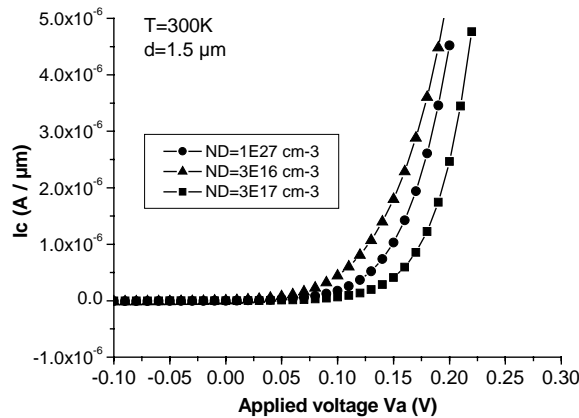


Fig. 3 : Current voltage characteristic versus active zone doping level at 300 K.

From these characteristics we have calculated the R_0A product (Fig.4).

As we can see on Fig. 4, this product presents a low variation versus the active zone thickness, excepted when this thickness becomes lower than $0.25 \mu m$. We can explain that if we consider the band gap energy given on Fig. 2. Indeed, the space charge zone is about $0.2\mu m$, when the SLs length is in the same order, all the active zone is depleted leading to a maximal R_0A value. Previously reported

elsewhere, we also verified that the R_0A product increases with the active zone doping level^[7].

5.b External quantum efficiency :

The effect of the active zone length on the performance is more notable concerning the quantum efficiency (Fig.5). These quantum efficiencies were calculated supposing an incident photon density of $10^{20} cm^{-2}$ at the photodetector surface ($y=0$), the absorption coefficient is done on Table 1.

For a given doping level, there is an optimum thickness, already between $1\mu m$ and $1.5\mu m$. This maximum could be relied to the electron diffusion length. In the case of an optimised active zone thickness and a doping level $N_D=3.10^{16} cm^{-3}$, quantum efficiency reach 25% in photovoltaic regime (0V polarisation). This value is in close agreement with recent experimental results performed on this type of photodetector structure [8]. When the active zone doping level increases, the quantum efficiency decreases, what can be explained by the increase of the recombination rate with the doping level.

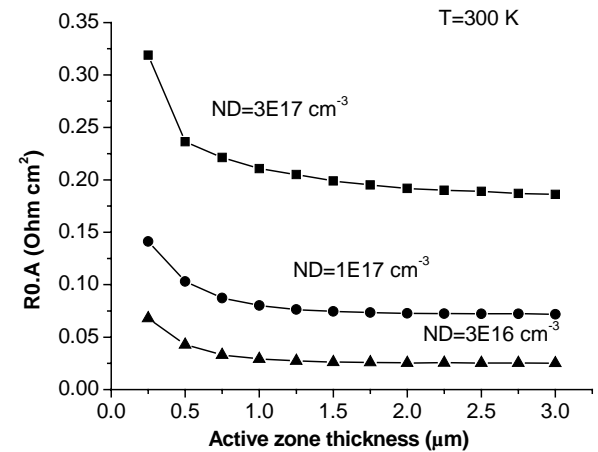


Fig. 4 : R_0A versus active zone thickness for three doping level at $T=300 K$.

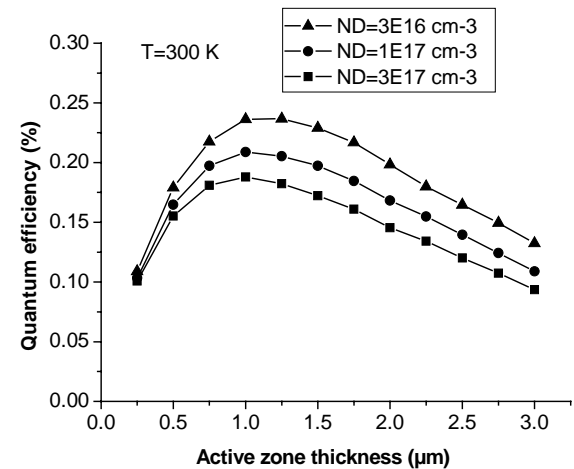


Fig. 5 : Quantum efficiency versus active zone thickness for three doping level at $T=300 K$

We can note that this result was obtained in the case of an isotropic active zone diffusion coefficient ($D_{par}=D_{per}$), this hypothesis is in fact not very realistic because of the multi layers morphology of the active zone. In order to take into account that, we give on figure 6 the calculation result obtained when the perpendicular diffusion coefficient is deviated by 10 and 100. As shown in the case of anisotropic D, the quantum efficiency value could be ten times weaker what is enormous (Fig. 6).

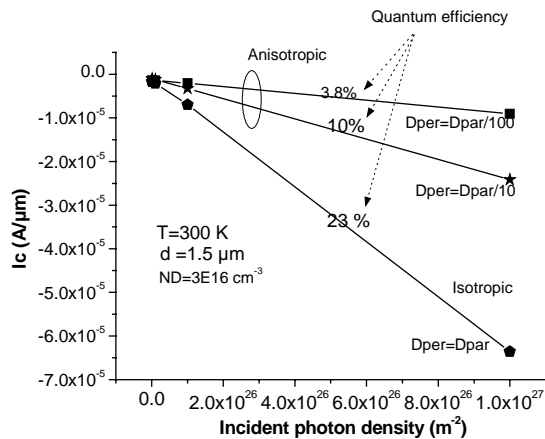


Fig. 6 : dependence of cathode current photodiode on incident photons density.

For this simulation D_{par} and D_{per} represent the diffusion coefficients respectively parallel and perpendicularly with surface diode. This simulation was obtained for an optimised active zone ($N_D=3.10^{16} \text{ cm}^{-3}$; $d=1,5 \mu\text{m}$).

5.c Specific detectivity :

The specific detectivity D_{λ}^* given by the relation (10) is a function of the $R_0.A$ product and the quantum efficiency given fig. 4 and fig. 5. Since the $R_0.A$ product is not very sensible to the active zone thickness, the shape of the specific detectivity D_{λ}^* is directly the same as the one from the quantum efficiency with a maximum about $1\mu\text{m}-1.3\mu\text{m}$ active zone widths.

The dependence of the detectivity on active zone width, for the three typical concentrations, is presented Fig 7. This theoretical detectivity is calculated for $\lambda = 4\mu\text{m}$. As a result, for the optimal active zone length and for a doping level of 3.10^{16}cm^{-3} , we obtain $D_{\lambda}^*=1.01 \cdot 10^9 \text{ cm W}^{-1} \text{ Hz}^{1/2}$. This value is one of the most expected value for RT operation and can be two times higher for an active zone doping level one decade more important.

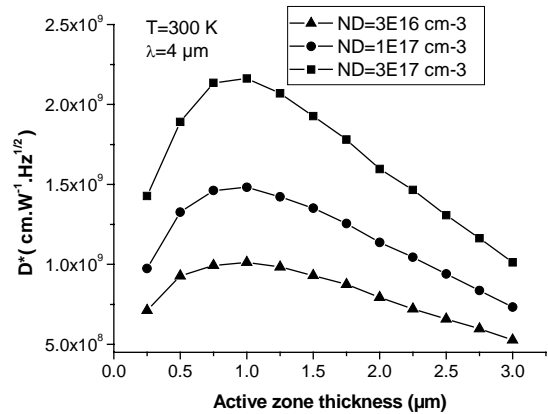


Fig. 7 : Theoretical specific detectivity D_{λ}^* for $T = 300 \text{ K}$ and $\lambda = 4\mu\text{m}$.

6. Conclusion :

In this paper a theoretical study of Sb-based photodetector performances at room temperature operation has been carried out by a FEMLAB modelling. Thanks to this modelling, we have demonstrated the strong influence of the active zone doping level on the $R_0.A$ product and of the active zone thickness on photodetector performances. The calculated results show the existence of an optimal active zone thickness in order to obtain a maximum detectivity. For our modelling conditions, depending on material parameters, this thickness seems to be about $1\mu\text{m}$ in the same order of electrons diffusion length in Sb-based systems. This result has to be confirmed by experimental measurements.

Consequently the modelling helps us to define the most appropriate geometry device to reach the highest photodetector performances. In next step, we could easily study the photodetector characteristics according to other geometrical parameters such as for example the components size or contact widths. We will also intend to study in a near future, the influence of surface states effects on components answer. Beyond this theoretical approach to define the accurate photodetector design, this FEMLAB modelling is also a support to help in the understanding and in the interpretation of the forthcoming realised photodetector characterization.

References

- [1] A. Rogalski, Prog. Quant. Electr. 27 (2003) 59.
- [2] A. Rogalski *et al*, Infrared Phys. Technol. To be published in 2005.
- [3] E. Rosencher and B Vinter "optoelectronique" Dunod Paris (2002).
- [4] J.B Rodriguez *et al*, J. Crystal Growth 274 (2005) 6.
- [5] FEMLAB Model library Comsol AB 2004.
- [6] Rodriguez *et al*, Physica E 28 (2005) 128.
- [7] G. Marre *et al*, Semicond. Sci. Technol. 18 (2003), 284.
- [8] Wei *et al*, Appl. Phys. Lett. 86 (2005) 233106.